



HAL
open science

Eddy Tracking in the Northwestern Indian Ocean During Southwest Monsoon Regimes

Corinne Trott, Bulusu Subrahmanyam, Alexis Chaigneau, Thierry Delcroix

► **To cite this version:**

Corinne Trott, Bulusu Subrahmanyam, Alexis Chaigneau, Thierry Delcroix. Eddy Tracking in the Northwestern Indian Ocean During Southwest Monsoon Regimes. *Geophysical Research Letters*, 2018, 45 (13), pp.6594-6603. 10.1029/2018GL078381 . hal-04430656

HAL Id: hal-04430656

<https://hal.science/hal-04430656>

Submitted on 1 Feb 2024

HAL is a multi-disciplinary open access archive for the deposit and dissemination of scientific research documents, whether they are published or not. The documents may come from teaching and research institutions in France or abroad, or from public or private research centers.

L'archive ouverte pluridisciplinaire **HAL**, est destinée au dépôt et à la diffusion de documents scientifiques de niveau recherche, publiés ou non, émanant des établissements d'enseignement et de recherche français ou étrangers, des laboratoires publics ou privés.

RESEARCH LETTER

10.1029/2018GL078381

Special Section:

New Understanding of the
Arabian Sea Circulation

Key Points:

- An eddy-tracking algorithm was applied to sea surface height in the northwestern Indian Ocean to examine eddy characteristics
- Summertime eddies are more numerous along the Arabian Peninsula but larger and more energetic in the Somali Current region
- Trajectories and characteristics of the Great Whirl are investigated from 1993 to 2014

Correspondence to:

C. B. Trott,
ctrott@seoe.sc.edu

Citation:

Trott, C. B., Subrahmanyam, B., Chaigneau, A., & Delcroix, T. (2018). Eddy tracking in the northwestern Indian Ocean during southwest monsoon regimes. *Geophysical Research Letters*, 45, 6594–6603. <https://doi.org/10.1029/2018GL078381>

Received 16 APR 2018

Accepted 9 JUN 2018

Accepted article online 19 JUN 2018

Published online 5 JUL 2018

Eddy Tracking in the Northwestern Indian Ocean During Southwest Monsoon Regimes

 Corinne B. Trott¹ , Bulusu Subrahmanyam¹ , Alexis Chaigneau^{2,3,4} , and Thierry Delcroix² 

¹School of the Earth, Ocean, and Environment, University of South Carolina, Columbia, SC, USA, ²LEGOS, University of Toulouse, CNES, CNRS, IRD, UPS, Toulouse, France, ³Institut de Recherches Halieutiques et Océanologiques du Bénin, Cotonou, Benin, ⁴International Chair in Mathematical Physics and Applications (UNESCO Chair), University of Abomey-Calavi, Cotonou, Benin

Abstract The northwestern Indian Ocean exhibits a relatively highly energetic eddy field during the southwest monsoon season between June and September. This study analyzes the seasonal and interannual variability of the eddy characteristics and their trajectories in the northwestern Indian Ocean using altimetric sea surface height observations from 1993 to 2014. Although the highest number of eddies is found in the Arabian Peninsula coastal region, the strongest eddies, characterized by large radii, amplitudes, and eddy kinetic energies are found along the Somali Current. Trajectories of anticyclonic and cyclonic eddies are investigated to provide insight on the generation and propagation of eddies of varying amplitudes. The largest annual eddy in the Somali Current system corresponds to the Great Whirl, for which the year-to-year variability with respect to shape, size, generation, and propagation was examined, as was the development of these characteristics over the Great Whirl's lifetime.

Plain Language Summary The ocean is full of highly energetic quasi-circular features known as mesoscale eddies having typical radii of 10–100 km. Eddies are significant transporters of global heat and ocean characteristics (like salinity and biodiversity). They are best observed by using satellite observations of fluctuations in sea surface height. In this study, we apply an algorithm to sea surface height satellite data in the northwestern Indian Ocean to better understand how and where eddies develop during the summer monsoon season, when eddies are strongest. We determined that though more eddies develop in the northern northwestern Indian Ocean, eddies with largest radii and amplitudes are found along the Somali Current region. These eddies in the Somali Current are also the most energetic, associated with stronger surface currents. The largest eddy observed in the Somali Current during the summer months is referred to as the Great Whirl. This research traces the location where the Great Whirl develops and propagates for each year from 1993 to 2014 and shows significant variability.

1. Introduction

Mesoscale eddies can be critical modulators of air-sea fluxes (Frenger et al., 2013; Ma et al., 2016; Villas-Boas et al., 2015) and transporters of seawater properties. The northwestern Indian Ocean (NIO) is a region of notable annual eddy generation during the southwest monsoon season (the boreal summer), characterized by strong regional southwesterly winds. The strongest low-level southwesterly monsoon jet is the Findlater jet blowing over the western Arabian Sea (Findlater, 1977). The Findlater jet synergizes with the topography of the Somali shoreline to induce conditions favorable for upper-level eddy generation by (i) the presence of Rossby waves (McCreary Jr et al., 1993), (ii) significant coastal upwelling (Trott et al., 2017), and (iii) barotropic instabilities (Jensen, 2001).

Rossby waves along 8°N directly influence the variability and patterns of sea level anomalies (SLAs) in the Arabian Sea. The impact of these waves on the coastal circulation of the Arabian Sea has been relatively well studied (McCreary Jr et al., 1993; Shankar & Shetye, 1997; Subrahmanyam et al., 2001). Brandt et al. (2002) attributed 87% of seasonal hydrographic variance in this region to first- and second-mode Rossby waves. These westward propagating waves generate at the western coastline of the Indian subcontinent and are continuously forced by wind stress curl over the Arabian Sea, hence their recurring annual signal (Brandt et al., 2002). Lighthill (1969) first predicted the 1-month lag time between the wind curl in May–June and the appearance of a northward Somali Current with accompanying eddies due to Rossby wave propagation. However, Leetmaa (1972) and Leetma (1973) factored in the direct influence of the Findlater Jet on the

Somali Current and found that wind-driven coastal upwelling was a more immediate influencer of summertime Somali Current and eddy generation.

The Findlater Jet induces negative summertime wind stress curl, resulting in coastal upwelling, approximately 5 °C cooler than the surrounding waters (Schott, 1983; Trott et al., 2017). Seo et al. (2008) analyzed the large summertime coastal sea surface temperature gradients in the western Arabian Sea and its connection to mesoscale activity. Coastal wind-induced vertical velocities on the order of 3 mm/day maintain baroclinic instability (Hurlburt & Thompson, 1976; Seo et al., 2008). The local eddy field strengthens during the southwest monsoon in an attempt to reestablish stratification (Boccaletti et al., 2007).

For the development of robust anticyclonic eddies such as the Great Whirl (GW) along the Somali Current, eddy generation is enhanced by barotropic instability. First suggested by Jensen (1991), the Somali Current advects waters with low potential vorticity northward. The large kinetic energy of the Somali Current enhances the lateral gradient in relative vorticity, generating barotropic instability and providing another generation mechanism for the GW (Seo, 2017).

As satellite altimetry provides sea surface height measurements at a high spatial and temporal scale, global eddy tracking has been of great interest. Thanks to the development of gridded data sets, composed of merged multimission altimeter data; several authors developed automatic eddy tracking algorithms applied to gridded sea surface height fields (Chaigneau et al., 2008; Chelton et al., 2011; Williams et al., 2011; Yi et al., 2014). Based on a global eddy tracking procedure, Chelton et al. (2011) revealed that nearly all of the eddies detected between 20°N and 20°S (including those in the Somali Current region) were nonlinear and, as such, are able to trap, transport, and redistribute physical and biogeochemical tracers. This nonlinear eddy behavior increases the complexity of understanding tropical eddies in comparison to their extratropical counterparts.

High-resolution satellite altimetry has been instrumental in our understanding of mesoscale eddy life cycles, for example, their development, propagation, and dissipation, and can provide insight to the Somali Current and its highly dynamic eddy field during the southwest monsoon season. Our objective is to apply an automatic eddy-tracking method to altimetric observations to better document and understand NIO eddies observed from 1993 to 2014, in particular during the SW monsoon. Characterizing NIO eddy dynamics is of great importance due to these eddies' impact on air-sea heat and moisture fluxes that determines rainfall over the Indian subcontinent (Vecchi et al., 2004).

2. Data and Methodology

Altimetric sea SLAs from merged multimission satellite observations are currently maintained and distributed by the Copernicus Marine and Environment Monitoring Service (marine.copernicus.eu) at a global horizontal grid resolution of 0.25° from 1993 to 2014. This daily data set incorporates a variety of altimeters (Ducet et al., 2000; Le Traon et al., 1998). SLAs, referenced to a 20-year mean from 1993 to 2012, were extracted in the NIO extending from 35°E–80°E to 10°S–30°N.

First, individual eddies, characterized by a center and an edge, were identified in SLA maps using the automated algorithm of Chaigneau et al. (2008, 2009). For each SLA map, this algorithm defines the anticyclonic eddy (AE) and cyclonic eddy (CE, respectively) centers as local SLA maxima (minima). The edge of each identified eddy is then determined as the outermost closed SLA contour around the detected centers (Chaigneau et al., 2008, 2009). To be retained as a valid eddy, the eddy edge must contain at least four connected SLA grid points, corresponding to a minimum radius of ~20 km. As mentioned by Pegliasco et al. (2015), detected eddies having small radii (20–40 km) or weak amplitudes (less than 1–2 cm) should probably be considered as noisy artifact structures on the daily SLA maps. However, this threshold-free method, that is very similar to that used in Chelton et al. (2011), has been shown to detect fewer false eddies than other commonly used methods (Chaigneau et al., 2008; Souza et al., 2011; Yi et al., 2014).

Second, eddy trajectories were constructed from these individual eddies using the tracking algorithm described in details in Pegliasco et al. (2015). For each eddy (e_1) identified on a given SLA map at time t_1 and delimited by a closed SLA contour C_1 , and for each eddy (e_2 , delimited by C_2) identified on the next map at time t_2 and intersecting e_1 while rotating in the same sense, a cost function (CF) is computed as

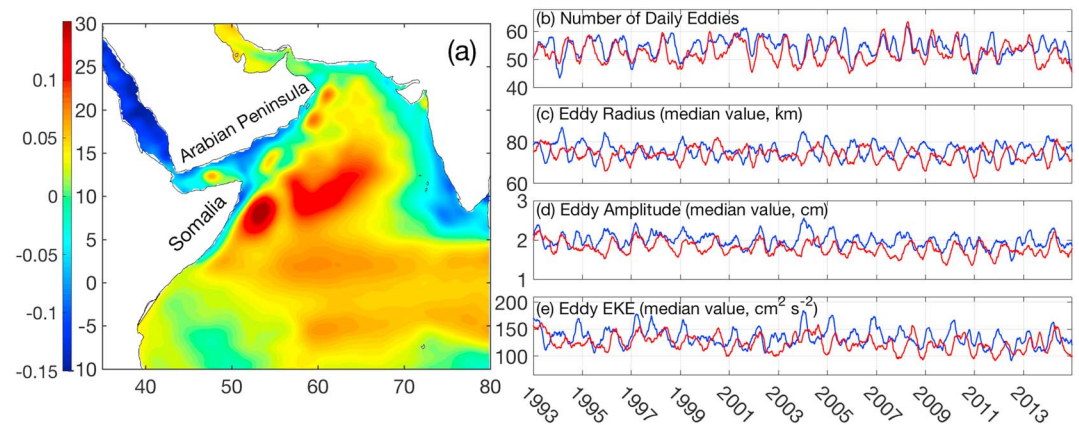


Figure 1. (a) Mean SLA during summer (in centimeter). Evolution of the eddy characteristics in the NIO from 1993 to 2014 for both CEs (in blue) and AEs (in red). (b) Number of eddies, (c) eddy radius, (d) eddy amplitude, and (e) eddy EKE. The time series are derived from daily data in region (a) smoothed with a 90-day running mean from 1993 to 2014.

$$CF_{e_1, e_2} = \sqrt{\left(\frac{\Delta R - \overline{\Delta R}}{\sigma_{\Delta R}}\right)^2 + \left(\frac{\Delta A - \overline{\Delta A}}{\sigma_{\Delta A}}\right)^2 + \left(\frac{\Delta EKE - \overline{\Delta EKE}}{\sigma_{\Delta EKE}}\right)^2} \quad (1)$$

where ΔR , ΔA , and ΔEKE are the differences in radius (R), amplitude (A), and eddy kinetic energy (EKE), respectively, between e_1 and any eddy e_2 intersecting e_1 (Pegliasco et al., 2015). The average departures ($\overline{\Delta R}$, $\overline{\Delta A}$, and $\overline{\Delta EKE}$) and the associated standard deviations ($\sigma_{\Delta R}$, $\sigma_{\Delta A}$, and $\sigma_{\Delta EKE}$) were determined from thousands of trajectory parts composed exclusively of single intersections between C_1 and C_2 . The algorithm selects the eddy at time t_2 that minimizes the CF and considers the eddy pair (e_1, e_2) to be the same eddy that is tracked from t_1 to t_2 . If no intersection is found between e_1 and any eddy e_2 , the eddy e_1 is considered as dissipated and the trajectory is stopped.

In contrast to other tracking methods based on distance criteria (e.g., Chaigneau et al., 2008; Chelton et al., 2011) this algorithm has the advantage to be threshold free and hence does not necessitate the choice of any arbitrary criterion, such as those found in Chelton et al. (2011), which does not include eddies with lifetimes shorter than 4 weeks. Additionally, another advantage of the Pegliasco et al. (2015) algorithm provides a more accurate shape of the eddy, rather than a central point and a mean radius. This then permits for observation-based studies for the vertical structure of eddies, which requires an exact eddy shape. However, the algorithm we apply can only be applied to SLA products having relatively high temporal resolution, ensuring that between two consecutive time steps the eddy contours intersect (e.g., the eddies have not traveled more than their typical radii).

3. Results

Between 1993 and 2014, the NIO eddy characteristics reveal a strong seasonality regarding number of eddies, radius, amplitude, and EKE (Figure 1). This seasonality is related to the strong summertime low-level jet that generates eddying (Flagg & Kim, 1998; McCreary et al., 1989), which dominates surface current variability from June through September (Lee et al., 2000). Eddy generation also occurs during winter as a response to the northeast monsoon, but with lower EKEs due to the weaker wind forcing (Schott & McCreary Jr, 2001). For much of the year, the NIO is populated by a higher number of CEs (average of 54.6, standard deviation of 5.4) than AEs (average \pm one standard deviation of 52.0 ± 5.0 ; Figure 1b). During June–September, coastal upwelling is strongest, resulting in negative SLA likely responsible for the higher number of CEs.

To study more thoroughly the eddy characteristics' seasonality in the NIO, we computed the monthly mean year of the eddy properties shown in Figure 1 (Figure 2). A Wilcoxon rank sum test (Haynes, 2013) between all paired time series in Figures 1 and 2 rejected the null hypothesis that the medians of AEs and CEs are equal at the 1% significance level. The number of AEs and CEs peaks at the onset of the summer monsoon season,

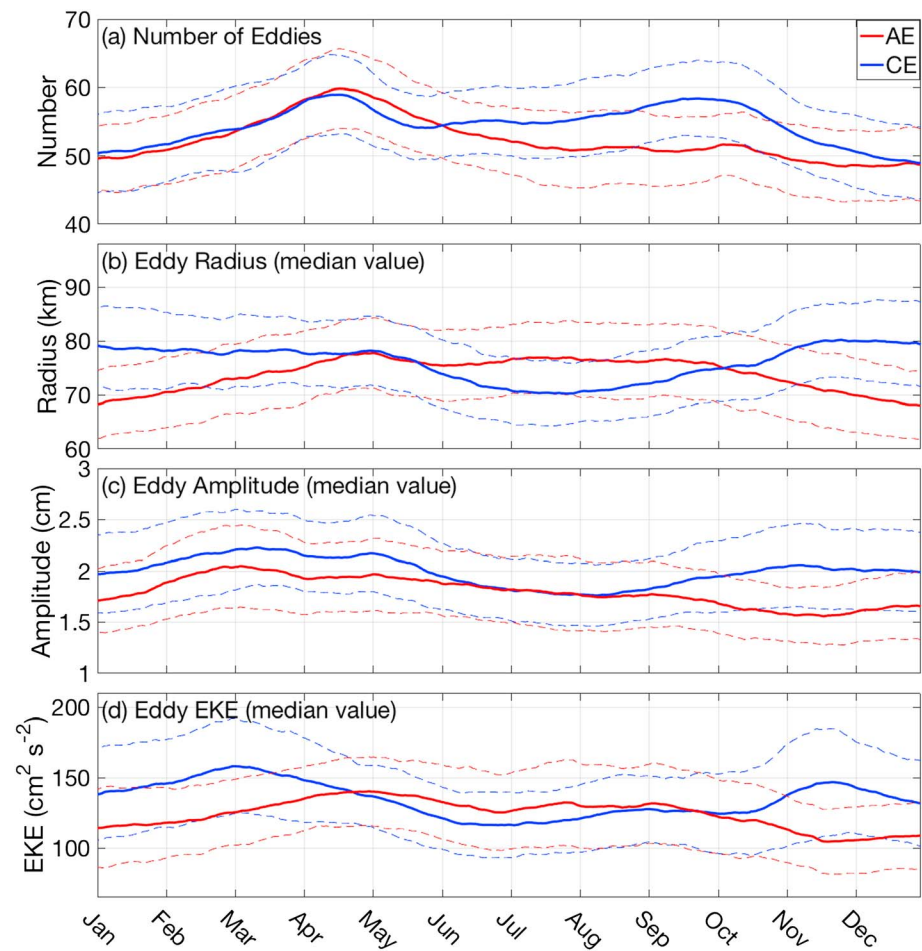


Figure 2. Mean seasonal cycle (solid lines) and \pm one standard deviation around the mean (dashed lines) of the eddy characteristics shown in Figure 1. EKE = eddy kinetic energy.

likely due to the increase of wind-driven instability, though the number of AEs drops below that of CEs for the rest of the year (Figure 2a). After this peak, the median radius, amplitude, and EKE of CEs reach an annual minimum in July–August (Figures 2b–2d). The median radius of CEs is larger than AEs in the NIO (particularly prior to 1997 and after 2003; Figure 1c), except during summer (Figure 2b). During the summer monsoon, CEs are most numerous and have smaller radii than AEs, though the difference between these distributions (and that of EKE) is within one standard deviation (Figures 2a and 2b). In contrast, median amplitude is similar for CEs and AEs during summer, but CEs are on average characterized by slightly higher amplitudes during the rest of the year (Figures 1d and 2c). The median radius and EKE of AEs are highest during the summer monsoon and comparable to the ship drift EKE estimates in Shenoi et al. (1999), when median amplitude is the same (Figures 2c and 2d). The spatial distribution of eddy amplitude is further explored in Figures 3e and 3f.

Figures 3a and 3b show that more eddies are observed along the Arabian Peninsula coastal ocean region (heretofore referred to as the Arabian Peninsula) than along the Somali Current region. However, eddies in the Somali Current region are larger in terms of radius and amplitude (Figures 3c–3f). Eddies with the largest mean radius were AEs located at approximately 54°E and 8°N (Figure 3c), consistent with observations of the GW (Beal & Donohue, 2013). The region of largest CE radii is located east of the AE radius maxima (Figure 3d), like the trajectories seen in Figure 4h where CEs are advected about the eastern boundary of the GW. The mean amplitude and EKE of CEs in the Somali Current region is greater than that of AEs (Figures 3e–3h). The peak mean amplitude for AEs (CEs) in the Somali Current region and along the Arabian Peninsula is 15.5 cm (18.1 cm) and 14.4 cm (10.1 cm), which is notably higher than the average mean SLA of 1.8 cm in

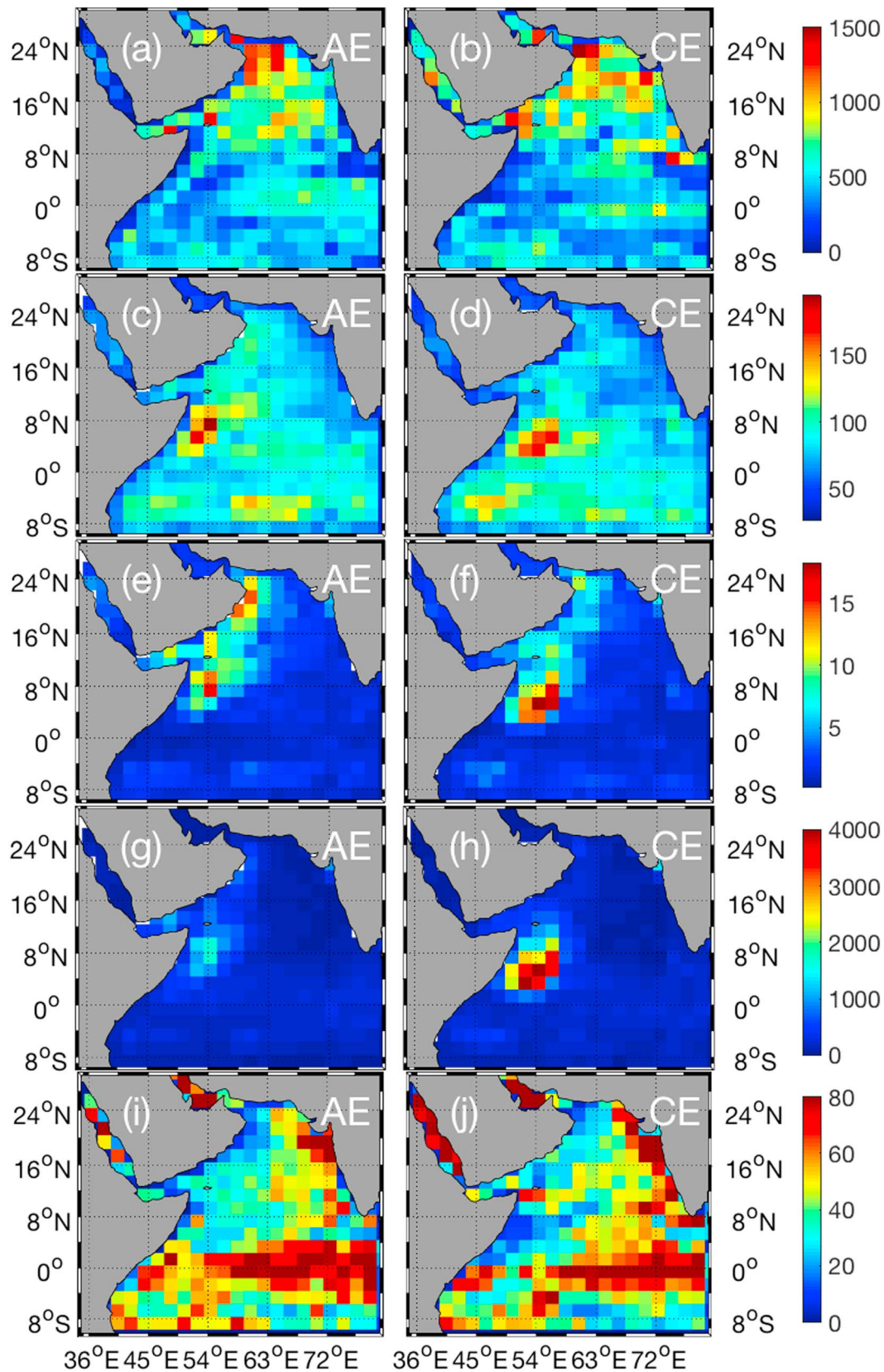


Figure 3. Mean spatial distribution of eddy characteristics during summer monsoon season (June–September) for AEs (left column) and CEs (right column). (a and b) Number of eddies; (c and d) radius (in kilometer), (e and f) amplitude (in centimeter), (g and h) EKE (in cm^2/s^2), and (i and j) number of eddy generation.

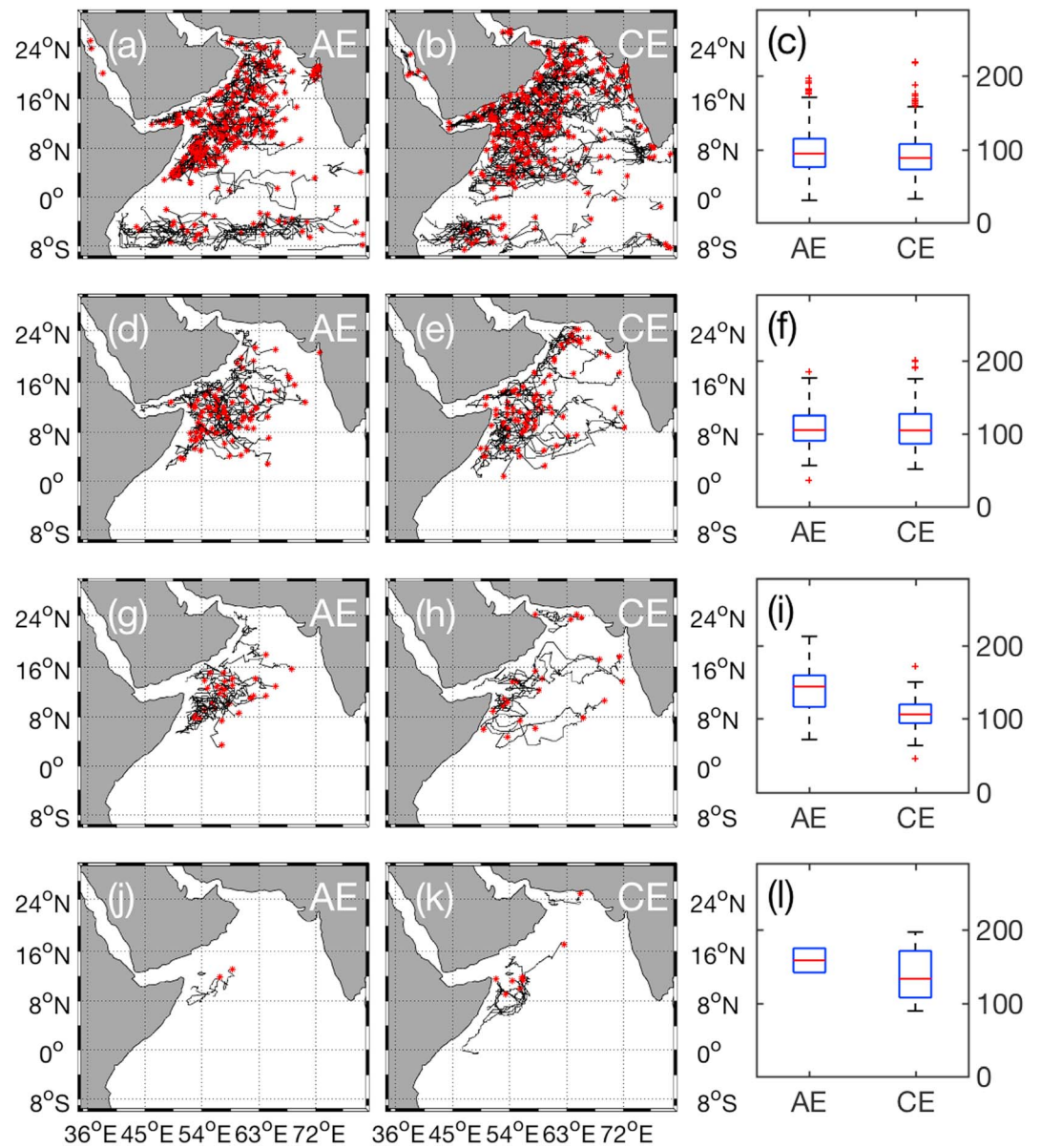


Figure 4. Trajectories of (left column) AEs and (right column) CEs generated during summer monsoon season (June to September) from 1993 to 2014 with maximum amplitudes ranging between (a and b) 10 and 20 cm, (d and e) 20 and 30 cm, (g and h) 30 and 40 cm, and (j and k) > 40 cm. Red asterisks correspond to the generation location of each trajectory. Boxplots show the distribution of mean eddy radius (in kilometer) for the trajectories plotted in Figures 4a–4h.

Figure 1a (Figures 3e–3f). During summer SW monsoon, the region of the highest EKE is undoubtedly the Somali Current region (Figures 3g and 3h). The highest mean CE EKE is $\sim 4,000 \text{ cm}^2/\text{s}^2$ while that for AEs is only $\sim 1,600 \text{ cm}^2/\text{s}^2$, which is characteristic for western boundary currents (Wyrki et al., 1976; Figures 3g–3h). The distribution of eddy generation (which is similar to that of the distribution of eddy dissipation, not shown) is primarily equatorial and along the west coast of India, though this signal is likely dominated by short-lived eddies (Figures 3i–3j). The distribution of eddy generation is similar between AEs and CEs, but there is more AE generation along the Somali Current than that of CEs (Figures 3i–3j). Trajectories of these highly energetic eddies are shown in Figure 4. As the number of eddies is counted each time an eddy travels into a new pixel, the ratio between Figures 3a and 3b and Figures 3i and 3j can provide some insight into the movement of AEs and CEs. After filtering to ensure eddies are not incorrectly counted twice when they do not move pixels, the sum of all pixels in Figures 3a (149,908), 3b (149,913), 3i (13,617), and

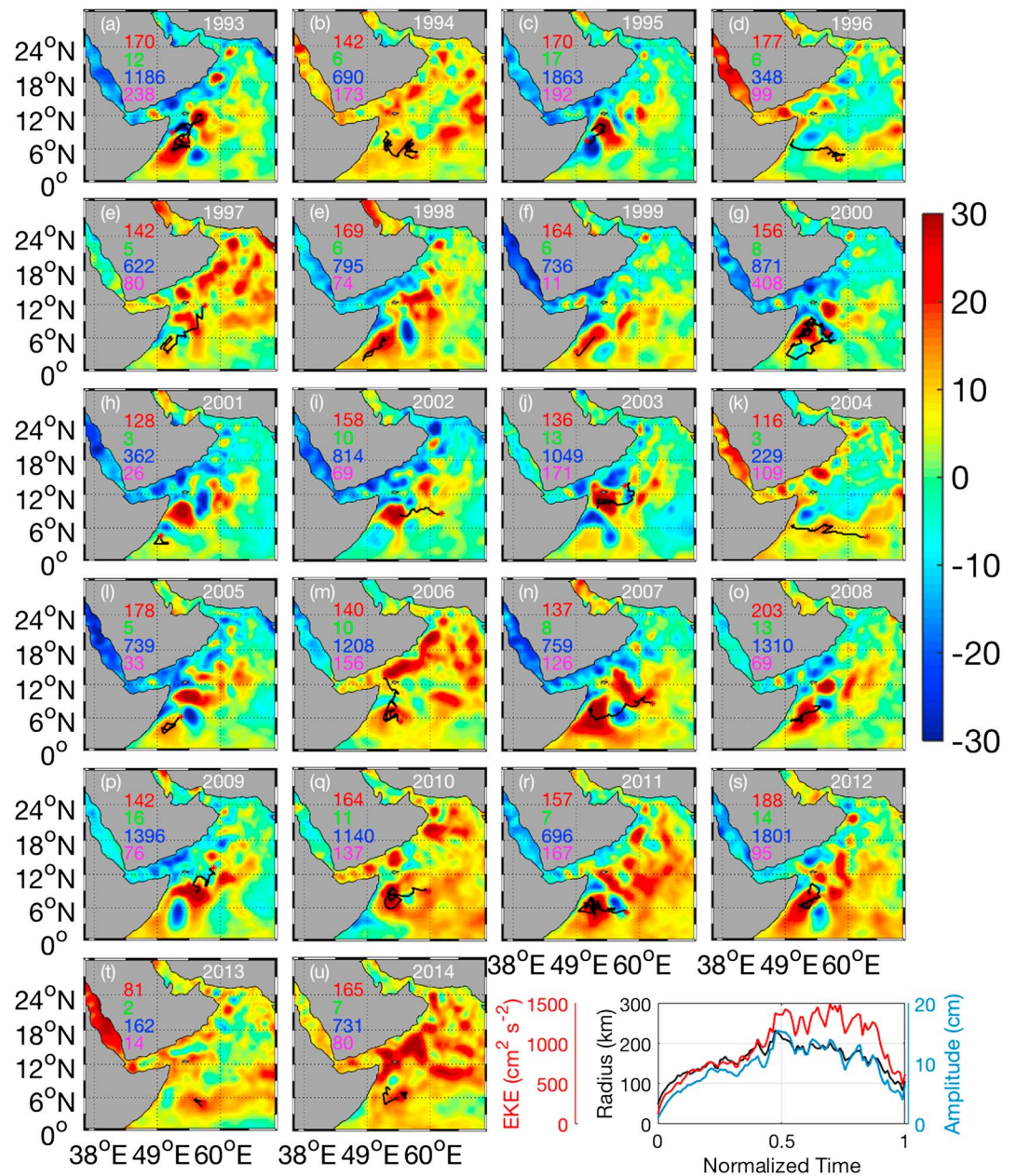


Figure 5. (a–u) Trajectories of the AE having the largest maximum radius in the Arabian Sea for each year between 1993 and 2014 and SLA (color shading, in cm) of the day corresponding to the largest GW radius. Trajectories that are in black and red asterisks signify the generation location of each eddy track. Mean radius (in kilometer) is in red text, mean amplitude (in centimeter) is in green text, mean EKE (in cm^2/s^2) is in blue text, and lifetime (in days) is in magenta text. Bottom right panel shows the ensemble mean radius, EKE, and amplitude for the 18 GW having a life span greater than 50 days. EKE = eddy kinetic energy; SLA = sea level anomaly; GW = Great Whirl.

3j (12,989), we determine that each AE trajectory contributes an average of 11.01 points in Figure 3a and each CE trajectory contributes an average of 11.54 points in Figure 3b.

During the summer monsoon, a greater rate of eddy generation takes place along the Arabian Peninsula than in the Somali Current region for both AEs and CEs with maximum amplitudes of 10–20 cm (Figures 4a and 4b). Between 8°S and the equator, eddies with amplitudes of 10–20 cm propagate westward along the path of the South Equatorial Current (Shankar et al., 2002). During the SW monsoon, CEs of amplitudes 10–20 cm also generate near the southernmost point of India at 8°N (Figure 4b). These eddies are probably generated

by Rossby waves triggered by upwelling Kelvin waves (McCreary Jr et al., 1993; Shankar et al., 2002; Subrahmanyam et al., 2001).

AEs and CEs having maximum amplitudes of 20–30 cm are highly concentrated in the Somali Current region and are less frequently generated along the Arabian Peninsula (Figures 4d and 4e). The distribution of mean radius of the trajectories shows larger radii for AEs than CEs in the 30–40 cm amplitude range (Figure 4i). For eddies having maximum amplitudes above 40 cm, CEs along the Somali Current region tend to propagate in a clockwise trajectory as they displace about the larger-radius AEs (Jensen, 1991; Matsuura & Yamagata, 1982). Akuetevi et al. (2016) describes this phenomenon of an asymmetric dipole where smaller cyclonic eddies generated by cyclonic vorticity *bursts* characteristic of a low-latitude western boundary current circle about their larger-radius counterparts (AEs). During the 22-year period of study, more CE trajectories (seven) than AE trajectories (two) were observed with maximum amplitudes greater than 40 cm (Figures 4j and 4k). In general, AEs have shorter average life spans compared to CEs for all amplitude ranges (44, 82, 120, and 95 days for AEs and 68, 91, 170, and 141 days for CEs with maximum amplitudes of, respectively, 10–20, 20–30, 30–40, and > 40 cm).

The anticyclonic GW has long been a feature of interest due to its consistent annual development and strength (Beal & Donohue, 2013; Findlay, 1876). In order to study its annual variability, Figure 5 shows the yearly trajectory of the AE having the largest radius in the region located north of the equator and west of 65°E. Eddy radii observed in this study are larger than that of Vic et al. (2014) as these authors arbitrarily determined the eddy edge as an isocontour of SLA of +6 cm, which led to GW radii of ~180 km. Of the 22 years plotted in Figure 5, the GW was present during the summer monsoon season 19 times and prior to the summer monsoon in 1996, 2004, and 2013, which, due to the observed westward propagation, weak mean EKEs, and consistent latitude, is likely due to downwelling Rossby waves (Brandt et al., 2002). The GW exhibited the largest size (maximum radius of 370–380 km) in 1993, 2007, and 2011, whereas the smallest maximal radii of 260–300 km were observed in 2002, 2009, and 2014. These three latter years correspond to weak monsoon years (Trott et al., 2017). The algorithm instead detected the Southern Gyre in some years rather than the GW (2001 and 2005). The decreased size of the maximum radius of the GW in weak monsoon years may be due to the weaker Findlater jet, leading to reduced wind-induced surface turbulence, which would be an interesting relationship to explore in future research (Trott et al., 2017). The GW formation and the direction of propagation strongly vary year to year (Figure 5) with no clear relationship to monsoon strength or other climatic events such as the El Niño Southern Oscillation or the Indian Ocean Dipole. To better understand the development of the GW, ensemble means were generated of the radius, amplitude, and EKE of the GW for years with life span greater than 50 days to eliminate short-lived eddies or classifications of the Southern Gyre rather than the GW, like in 2001 and 2005 (Figure 5; Samelson et al., 2014). We note that the GW matures halfway throughout its life cycle for amplitude and radius and peaks with respect to EKE about 70% into its life cycle. There is a strong decrease of these properties during the last 30% of the GW's life cycle (Figure 5).

4. Conclusion

We have applied an eddy identification and tracking algorithm to a 22-year (1993–2014) daily SLA data set to study the characteristics (radius, amplitude, and EKE) and variability of eddies in the NIO. Long-term and seasonal eddy generation in the NIO, as a response to monsoonal forcing on the surface current variability, was investigated, quantifying the statistically different characteristics of AEs and CEs. As wind magnitude, Somali Current strength, and eddy robustness peaks during the summer SW monsoon season, a special emphasis was given to the trajectories and characteristics of eddies generated between June and September. The trajectories of these eddies reveal diverse distribution of AEs and CEs depending of their maximum amplitudes. This study concludes that in the Somali Current region during the summer monsoon, AEs are, on average, larger in size, whereas CEs have higher amplitudes and EKE. During the same season but off the Arabian Peninsula, AEs tend to be more numerous, larger in size, and have a higher amplitude. The majority of eddies are found in the northern Arabian Sea, but the strongest eddies are in the Somali Current outflow region. We compared the number of eddies and eddy characteristic such as median radius, median amplitude, and median EKE temporally to compare the stark difference between eddies during the summer monsoon season compared to the rest of the year. We traced the trajectory of the GW to observe

annual changes in its development and propagation. The GW showed high variability in its location of generation and direction of trajectory and its maximal radius varied from 260 km in 2002 to 380 km in 1993.

Acknowledgments

This work is supported by the ONR NASCar (Northern Arabian Sea Circulation-autonomous research) award N00014-17-1-2468 awarded to B. S. Multimission altimetry data are available via Copernicus Marine Environment Monitoring Service (CMEMS; marine.copernicus.eu). The authors would like to thank the anonymous reviewers and the Editor, whose comments significantly contributed to the improvement of this paper.

References

- Akueteve, C. Q. C., Barnier, B., Verron, J., Molines, J. M., & Lecomte, A. (2016). Interactions between the Somali Current eddies during the summer monsoon: Insights from a numerical study. *Ocean Science*, *12*(1), 185–205. <https://doi.org/10.5194/os-12-185-2016>
- Beal, L. M., & Donohue, K. A. (2013). The Great Whirl: Observations of its seasonal development and interannual variability. *Journal of Geophysical Research: Oceans*, *118*, 1–13. <https://doi.org/10.1029/2012JC008198>
- Boccaletti, G., Ferrari, R., & Fox-Kemper, B. (2007). Mixed layer instabilities and restratification. *Journal of Physical Oceanography*, *37*(9), 2228–2250. <https://doi.org/10.1175/JPO3101.1>
- Brandt, P., Stramma, L., Schott, F., Fischer, J., Dengler, M., & Quadfasel, D. (2002). Annual Rossby waves in the Arabian Sea from TOPEX/POSEIDON altimeter and in situ data. *Deep Sea Research Part II: Topical Studies in Oceanography*, *49*(7–8), 1197–1210. [https://doi.org/10.1016/S0967-0645\(01\)00166-7](https://doi.org/10.1016/S0967-0645(01)00166-7)
- Chaigneau, A., Eldin, G., & Dewitte, B. (2009). Eddy activity in the four major upwelling systems from satellite altimetry (1992–2007). *Progress in Oceanography*, *83*(1–4), 117–123. <https://doi.org/10.1016/j.pocean.2009.07.012>
- Chaigneau, A., Gizolme, A., & Grados, C. (2008). Mesoscale eddies off Peru in altimeter records: Identification algorithms and eddy spatio-temporal patterns. *Progress in Oceanography*, *79*(2–4), 106–119. <https://doi.org/10.1016/j.pocean.2008.10.013>
- Chelton, D. B., Schlax, M. G., & Samelson, R. M. (2011). Global observations of nonlinear mesoscale eddies. *Progress in Oceanography*, *91*(2), 167–216. <https://doi.org/10.1016/j.pocean.2011.01.002>
- Ducet, N., Le Traon, P. Y., & Reverdin, G. (2000). Global high-resolution mapping of ocean circulation from TOPEX/Poseidon and ERS-1 and-2. *Journal of Geophysical Research*, *105*(C8), 19,477–19,498. <https://doi.org/10.1029/2000JC900063>
- Findlater, J. (1977). A numerical index to monitor the Afro-Asian monsoon during the northern summers. *Meteorological Magazine*, *106*, 170–184.
- Findlay, A. G. (1876). *A directory for the navigation of the Indian Ocean: With descriptions of its coasts, islands, etc., from Cape of Good Hope to the Strait of Sunda and western Australia, including also the Red Sea and the Persian Gulf; the winds, monsoons, and currents, and the passages from Europe to its various ports*. London: Richard Holmes Laurie.
- Flagg, C. N., & Kim, H. S. (1998). Upper ocean currents in the northern Arabian Sea from shipboard ADCP measurements collected during the 1994–1996 US JGOFS and ONR programs. *Deep Sea Research Part II: Topical Studies in Oceanography*, *45*(10–11), 1917–1959. [https://doi.org/10.1016/S0967-0645\(98\)00059-9](https://doi.org/10.1016/S0967-0645(98)00059-9)
- Frenger, I., Gruber, N., Knutti, R., & Münnich, M. (2013). Imprint of Southern Ocean eddies on winds, clouds and rainfall. *Nature Geoscience*, *6*(8), 608–612. <https://doi.org/10.1038/ngeo1863>
- Haynes, W. (2013). Wilcoxon rank sum test. In *Encyclopedia of systems biology* (pp. 2354–2355). New York: Springer.
- Hurlburt, H. E., & Thompson, J. D. (1976). A numerical model of the Somali Current. *Journal of Physical Oceanography*, *6*(5), 646–664. [https://doi.org/10.1175/1520-0485\(1976\)006<0646:ANMOTS>2.0.CO;2](https://doi.org/10.1175/1520-0485(1976)006<0646:ANMOTS>2.0.CO;2)
- Jensen, T. G. (1991). Modeling the seasonal undercurrents in the Somali Current system. *Journal of Geophysical Research*, *96*(C12), 22,151–22,167. <https://doi.org/10.1029/91JC02383>
- Jensen, T. G. (2001). Arabian Sea and Bay of Bengal exchange of salt and tracers in an ocean model. *Geophysical Research Letters*, *28*(20), 3967–3970. <https://doi.org/10.1029/2001GL013422>
- Le Traon, P. Y., Nadal, F., & Ducet, N. (1998). An improved mapping method of multisatellite altimeter data. *Journal of Atmospheric and Oceanic Technology*, *15*(2), 522–534. [https://doi.org/10.1175/1520-0426\(1998\)015<0522:AIMMOM>2.0.CO;2](https://doi.org/10.1175/1520-0426(1998)015<0522:AIMMOM>2.0.CO;2)
- Lee, C. M., Jones, B. H., Brink, K. H., & Fischer, A. S. (2000). The upper-ocean response to monsoonal forcing in the Arabian Sea: Seasonal and spatial variability. *Deep Sea Research Part II: Topical Studies in Oceanography*, *47*(7–8), 1177–1226. [https://doi.org/10.1016/S0967-0645\(99\)00141-1](https://doi.org/10.1016/S0967-0645(99)00141-1)
- Leetmaa, A. (1972). The response of the Somali Current to the southwest monsoon of 1970. *Deep Sea Research and Oceanographic Abstracts*, *19*, 319–325. [https://doi.org/10.1016/0011-7471\(72\)90025-3](https://doi.org/10.1016/0011-7471(72)90025-3)
- Leetmaa, A. (1973). The response of the Somali current at 2°S to the southwest monsoon of 1971. *Deep Sea Research and Oceanographic Abstracts*, *20*, 397–400. [https://doi.org/10.1016/0011-7471\(73\)90062-4](https://doi.org/10.1016/0011-7471(73)90062-4)
- Lighthill, M. J. (1969). Unsteady wind-driven ocean currents. *Quarterly Journal of the Royal Meteorological Society*, *95*(406), 675–688. <https://doi.org/10.1002/qj.49709540602>
- Ma, X., Jing, Z., Chang, P., Liu, X., Montuoro, R., Small, R. J., et al. (2016). Western boundary currents regulated by interaction between ocean eddies and the atmosphere. *Nature*, *535*(7613), 533–537. <https://doi.org/10.1038/nature18640>
- Matsuura, T., & Yamagata, T. (1982). On the evolution of nonlinear planetary eddies larger than the radius of deformation. *Journal of Physical Oceanography*, *12*(5), 440–456. [https://doi.org/10.1175/1520-0485\(1982\)012<0440:OTEONP>2.0.CO;2](https://doi.org/10.1175/1520-0485(1982)012<0440:OTEONP>2.0.CO;2)
- McCreary, J. P., Lee, H. S., & Enfield, D. B. (1989). The response of the coastal ocean to strong offshore winds: With application to circulations in the Gulfs of Tehuantepec and Papagayo. *Journal of Marine Research*, *47*(1), 81–109. <https://doi.org/10.1357/002224089785076343>
- McCreary, J. P. Jr., Kundu, P. K., & Molinari, R. L. (1993). A numerical investigation of dynamics, thermodynamics and mixed-layer processes in the Indian Ocean. *Progress in Oceanography*, *31*(3), 181–244. [https://doi.org/10.1016/0079-6611\(93\)90002-U](https://doi.org/10.1016/0079-6611(93)90002-U)
- Pegliasco, C., Chaigneau, A., & Morrow, R. (2015). Main eddy vertical structures observed in the four major eastern boundary upwelling systems. *Journal of Geophysical Research: Oceans*, *120*, 6008–6033. <https://doi.org/10.1002/2015JC010950>
- Samelson, R. M., Schlax, M. G., & Chelton, D. B. (2014). Randomness, symmetry, and scaling of mesoscale eddy life cycles. *Journal of Physical Oceanography*, *44*(3), 1012–1029. <https://doi.org/10.1175/JPO-D-13-0161.1>
- Schott, F. (1983). Monsoon response of the Somali Current and associated upwelling. *Progress in Oceanography*, *12*(3), 357–381. [https://doi.org/10.1016/0079-6611\(83\)90014-9](https://doi.org/10.1016/0079-6611(83)90014-9)
- Schott, F. A., & McCreary, J. P. Jr. (2001). The monsoon circulation of the Indian Ocean. *Progress in Oceanography*, *51*(1), 1–123. [https://doi.org/10.1016/S0079-6611\(01\)00083-0](https://doi.org/10.1016/S0079-6611(01)00083-0)
- Seo, H. (2017). Distinct influence of air–sea interactions mediated by mesoscale sea surface temperature and surface current in the Arabian Sea. *Journal of Climate*, *30*(20), 8061–8080. <https://doi.org/10.1175/JCLI-D-16-0834.1>
- Seo, H., Murtugudde, R., Jochum, M., & Miller, A. J. (2008). Modeling of mesoscale coupled ocean–atmosphere interaction and its feedback to ocean in the western Arabian Sea. *Ocean Modelling*, *25*(3–4), 120–131. <https://doi.org/10.1016/j.ocemod.2008.07.003>
- Shankar, D., & Shetye, S. R. (1997). On the dynamics of the Lakshadweep high and low in the southeastern Arabian Sea. *Journal of Geophysical Research*, *102*(C6), 12,551–12,562. <https://doi.org/10.1029/97JC00465>

- Shankar, D., Vinayachandran, P. N., & Unnikrishnan, A. S. (2002). The monsoon currents in the north Indian Ocean. *Progress in Oceanography*, 52(1), 63–120. [https://doi.org/10.1016/S0079-6611\(02\)00024-1](https://doi.org/10.1016/S0079-6611(02)00024-1)
- Shenoi, S. S. C., Saji, P. K., & Almeida, A. M. (1999). Near-surface circulation and kinetic energy in the tropical Indian Ocean derived from Lagrangian drifters. *Journal of Marine Research*, 57(6), 885–907. <https://doi.org/10.1357/002224099321514088>
- Souza, J. M. A. C. D., De Boyer Montegut, C., & Le Traon, P. Y. (2011). Comparison between three implementations of automatic identification algorithms for the quantification and characterization of mesoscale eddies in the South Atlantic Ocean. *Ocean Science*, 7(3), 317–334. <https://doi.org/10.5194/os-7-317-2011>
- Subrahmanyam, B., Robinson, I. S., Blundell, J. R., & Challenor, P. G. (2001). Indian Ocean Rossby waves observed in TOPEX/POSEIDON altimeter data and in model simulations. *International Journal of Remote Sensing*, 22(1), 141–167. <https://doi.org/10.1080/014311601750038893>
- Trott, C. B., Subrahmanyam, B., & Murty, V. S. N. (2017). Variability of the Somali Current and eddies during the southwest monsoon regimes. *Dynamics of Atmospheres and Oceans*, 79, 43–55. <https://doi.org/10.1016/j.dynatmoce.2017.07.002>
- Vecchi, G. A., Xie, S. P., & Fischer, A. S. (2004). Ocean–atmosphere covariability in the western Arabian Sea. *Journal of Climate*, 17(6), 1213–1224. [https://doi.org/10.1175/1520-0442\(2004\)017<1213:OCITWA>2.0.CO;2](https://doi.org/10.1175/1520-0442(2004)017<1213:OCITWA>2.0.CO;2)
- Vic, C., Roulet, G., Carton, X., & Capet, X. (2014). Mesoscale dynamics in the Arabian Sea and a focus on the Great Whirl life cycle: A numerical investigation using ROMS. *Journal of Geophysical Research: Oceans*, 119, 6422–6443. <https://doi.org/10.1002/2014JC009857>
- Villas-Boas, A. B., Sato, O. T., Chaigneau, A., & Castelão, G. P. (2015). The signature of mesoscale eddies on the air–sea turbulent heat fluxes in the South Atlantic Ocean. *Geophysical Research Letters*, 42, 1856–1862. <https://doi.org/10.1002/2015GL063105>
- Williams, S., Petersen, M., Bremer, P. T., Hecht, M., Pascucci, V., Ahrens, J., et al. (2011). Adaptive extraction and quantification of geophysical vortices. *IEEE Transactions on Visualization and Computer Graphics*, 17(12), 2088–2095. <https://doi.org/10.1109/TVCG.2011.162>
- Wyrski, K., Magaard, L., & Hager, J. (1976). Eddy energy in the oceans. *Journal of Geophysical Research*, 81, 2641–2646. <https://doi.org/10.1029/JC081i015p02641>
- Yi, J., Du, Y., He, Z., & Zhou, C. (2014). Enhancing the accuracy of automatic eddy detection and the capability of recognizing the multi-core structures from maps of sea level anomaly. *Ocean Science*, 10(1), 39–48. <https://doi.org/10.5194/os-10-39-2014>